Application of agricultural wastes of rice to lead removal from aqueous solution, study of equilibriums and kinetics

Khalilollah Moeinian[a,b], Roohollah Rostami[a,b], Tayyabeh Rastgoo[a,b], Seyed Mahmoud Mehdinia[b,*]

[a]*Research Center for Health Sciences and Technologies, School of Health, Semnan University of Medical Sciences, Semnan, Iran, email: khalilollah@semums.ac.ir (K. Moeinian), ro.rostamy@gmail.com (R. Rostami), t.rastgo57@gmail.com (T. Rastgoo)*
[b]*Department of Environmental Health Engineering, School of Health, Semnan University of Medical Sciences, Semnan, Iran, Tel. +989123325372, Fax +982335220140, email: smmehdinia@semums.ac.ir (S.M. Mehdinia)*

ABSTRACT

This study investigated the effect of organic base adsorbents derived from agricultural wastes; namely rice husk silica (RHS), raw rice husk (RRH), and rice bran (RB) on removing lead ions from aqueous solutions. RRH and RB are collected from the agricultural wastes of north of Iran farms and RHS prepared at 800ºC temperature after acid leaching. The adsorption rate examined in different contact times (CT from 5 to 90 min), initial pH (pH_0 = 5, 6, 7, 8 and 9), adsorbents dosages (AD = 0.5, 1 and 1.5 mg/L) and initial concentration of lead (C_0 = 1, 5, 10 and 15 mg/L). The optimum conditions for adsorption of lead were pH of 6, adsorbent dosage of 1 g/L and contact time of 60 min, and RHS showed maximum efficiency up to 96.4%. The results were admissibly confident with linear and non-linear Langmuir, Freundlich and pseudo first-order models. Langmuir isotherm indicated q_m for the RHS up to 15.6 mg/L compared to RRH with 7.3 mg/g and RB with 4.8 mg/g. Adsorption process in this system was limited by mainly sorption process and bulk or boundary layer diffusion. The dominant reaction was estimated to be the ion-exchange according to the obtained energy values of sorption.

Keywords: Environmental pollution; Rice husk; Water pollution; Lead ions

1. Introduction

Over the course of recent decades human activities have led to a considerable increase in environmental pollution, so there is a growing concern over environmental pollutions [1]. Heavy metals are some of these pollutants which have dangerous effects on human physiology when they exceed the tolerance levels. They are non-biodegradable, accumulate in living organisms, and cause different diseases [2]. Considering the methods to removal of heavy metals, adsorption is an effective and affordable technology specially for purification of low concentrations of contaminates [3].

Activated carbon generated from different materials is extensively used for heavy metals adsorption in the purification of aqueous solution. Since commercial activated carbon is not affordable in large scale, hence today, researchers have found inexpensive adsorbents instead of commercial activated carbon.

Lately, notable consideration is devoted to study heavy metals removal from aqueous solutions by using agricultural wastes such as wheat straw, rice husk and so on; for instance in a most recent work Mu et al., reported a successful experience on adsorption of lead by amended wheat straw [4]. In this line of research, wastes of rice and adsorbents derived from the wastes are investigated in recent years, because they are widely available and affordable materials [5–8]. This study aims to investigate adsorption effectiveness of, raw rice husk, and rice bran for the removal

---

*Corresponding author.

of lead ions from aqueous solutions. Extent study on the isotherms and kinetic aspects of the sorption process is raised to understand the adsorption characteristics.

2. Materials and methods

2.1. Preparation of the adsorbents

RRH and RB collected from the agricultural wastes of farms in the north of Iran and RHS was prepared as a method proposed previously [9]. In this regard, the RRH was rinsed several times with water to remove dirt and other contaminants, and then dried at 110°C for 12 h. After drying, 50 g of the RRH was subjected to 1 L of an acid solution, 3% (v/v) hydrochloric acid (HCl), 10% (v/v) sulfuric acid (H_2SO_4) and for 2 h to acidic amendment. After thoroughly rinsing with distilled water (DW), it was dried again for 4 h at 100°C, and calicinated in a static air muffle furnace for 4 h at 800°C.

2.2. Characterization of the adsorbents

Characteristics of the RRH and RHS were examined by studying surface morphology with scanning electron microscopy (SEM) in physics laboratory of Sharif University of Technology, Tehran. Moreover, the secured samples of the sorbents were sent to chemistry laboratory of Kharazmi University, Tehran for CHNS analysis. pHpzc was determined with pH-drift analysis as described by Lopez et al. [10], and the chemical functional groups of the sorbents were examined by FTIR (Termo Nicolet 6700). Specific surface area was determined by BET analysis by a ThermoFinnigan Sorptomatic apparatus using nitrogen adsorption at –196°C.

2.3. Adsorption experiments

250 ml batch reactors were used for all experiments and the procedures carried out at the normal temperature and pressure. Analytical-grade lead chloride (Merck Inc.), was used to prepare known concentrations of lead in distilled water. The adsorption rate was examined in different contact times (*CT* from 5 to 90 min), initial *pH* (pH_0 = 5, 6, 7, 8 and 9), adsorbents dosages (*AD* = 0.5, 1 and 1.5 mg/L) and initial concentration of lead (C_0 = 1, 5, 10 and 15 mg/L). Atomic absorption spectrometer, Perkin Elmer 100 was used for measurement of lead concentrations. Quality control of the experiment and measurements was performed by taking blank samples in each set of the experiments and replications for three times.

Data analyses achieved by using Excel solver add-Ins, and non-linear modelling performed by using Curve Expert 1.4. The correlation determination (R^2) and standard error (SE) were used to determine appropriateness of sorption isotherms and the examined models. R^2 values close to 1.0 and small SE values were considered to have better curve fitting.

3. Results and discussion

3.1. The adsorbents

A considerable reduction in carbon content was seen in RHS (0.09%) compared to RRH (35.92%). Also, the reduction of nitrogen and hydrogen content was resulted in RHS (Table 1). The large amount of carbon in RRH is related to organic materials in its structure, as RRH consist of almost 95% organic materials mainly including; α-cellulose 43.3%, Lignin 22%, D-xylose 17.52%, I-arabinose 6.53%, Mthylglucuronic acid 3.27% and D-galactose 2.37% [11]. The results
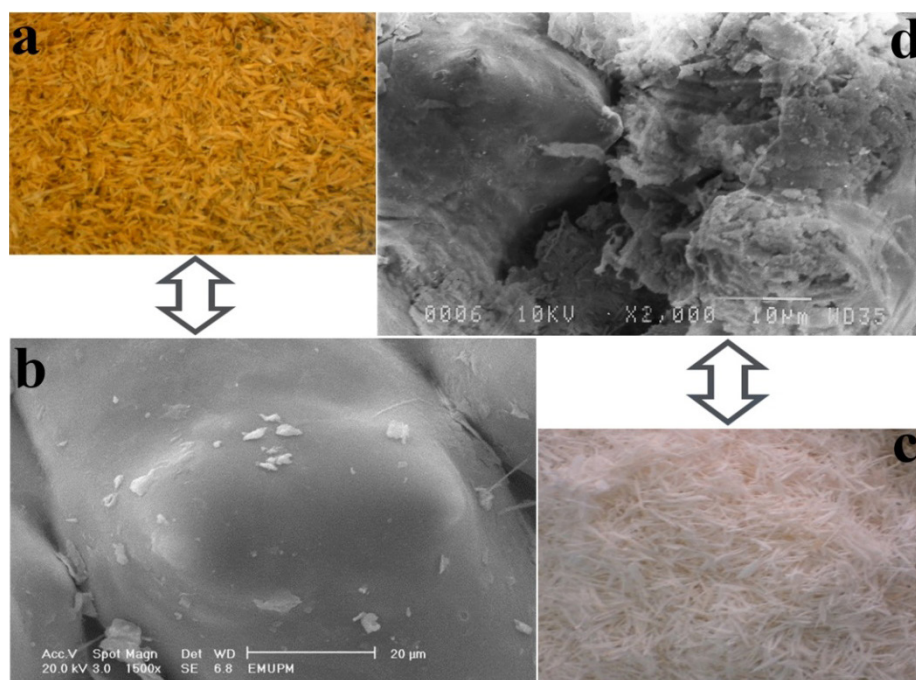
Fig. 1. RRH (a), SEM image of RRH (b), RHS (c), SEM image of RHS (d).

Table 1
Physical-chemical properties of the RRH & RHS

	Selected characteristics parameters					
	Density (g/L)	pH	C (%)	H (%)	N (%)	SiO$_2$ (%)
Raw rice husk (RRH)	93.3	6.7	35.92	4.84	0.42	NM*
Rice husk silica (RHS)	44.5	7.5	0.09	0.16	0.14	94.24

NM* = not measured

showed that SiO$_2$ (94.24%) was the main portion of RHS components. Likewise, the high values of SiO$_2$ in RHS were reported by Mehdinia et. al. (97.35%) and from 83.66 to 99.66%, depended on the preparation condition, by Yalcin et al. [12] and Mehdinia et al. [13]. While, the reported contents of SiO$_2$ for RRH (25.81 [12] and 20.2% [14]), and RB (3.34% [15]), were significantly lower than RHS.

High SiO$_2$ and lower carbon content of RHS show its mineral structure compared to RRH, which is mainly organic. This transmutation form RRH to RHS which occurred during the acidic treatment and calcination gives a higher stability and tolerant against biological degradation of RHS, as an adsorbent during the aquatic adsorption process. And the silicon dioxide molecules could make networks of SiO$_2$ in a crystalline structure [16].

Regarding to the FTIR spectra of the sorbents (Fig. 2), disulfide week bands (465 cm^{-1}) [17], C-H or S-OR esters (700–1200 cm^{-1}) also remarked as gel network [18,19], strong bending of C=S thyocarbonil or most probably broad, strong bending of Si-OR, and Si-O-Si siloxane (900–1400 cm^{-1}) [20], and strong Si-H silane bending (2360 cm^{-1}) [21] are extending in the RHS comparing with the RRH and RB. While the alkanes (2925 cm^{-1}) and alcohols (3418 cm^{-1}) are notably declined [20,22].

Finally, the resulted surface area for the RHS was obtained about 226.3 m^2·g^{-1}, by the BET analysis, with pore diameters mainly lower than 20 nm (supplementary material Fig. 1S and 2S). Also, the pH-drift analysis indicated pHpzc about 6.1 for RRH and RB, and 6.6 for RHS.

3.2. Effect of pH

The results showed the most removal efficiency (RE, Eq. (1)) of lead by using adsorbents in the initial solution pH of 6. RE of lead for RHS, RRH and RB were respectively 92.3%, 85.7% and 84.3% in pH 6.

$$RE\% = \frac{(C_0 - C_e) \times 100}{C_0} \qquad (1)$$

where C_0 is the initial concentration of lead, and C_e is the remained lead in the solution (mg/L).

Removal efficiency of lead from the solution in the pHs higher than 6 and in initial solution pH (pH$_0$) of 5 was decreased (see Fig. 3). This indicated that the most appropriate pH for adsorption of lead with all three adsorbents is 6. It is clear that in the higher pH values, lead and most heavy metals will precipitate with reduction of their solubility due to reaction with hydroxyl. A notable part of the total lead is present as a precipitate of Pb(OH)$_2$ from pH 7.7 to 11, which is not available for adsorption [23].
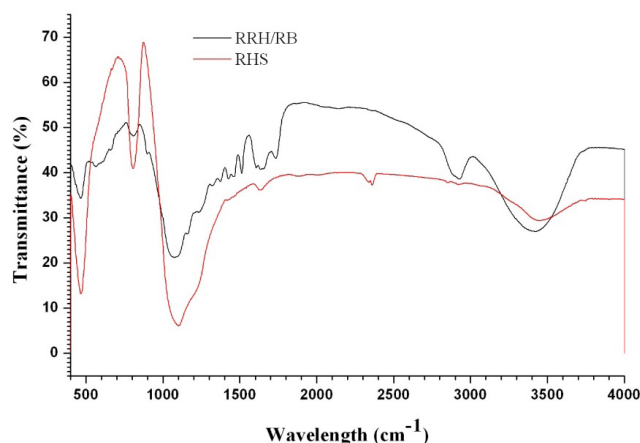
Fig. 2. FTIR spectra for the RRH, RB, and RHS.
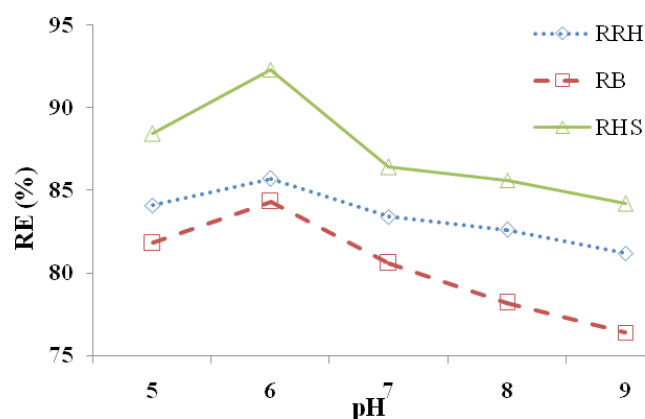
Fig. 3. Removal efficiency of lead in different pH values (AD = 1.0 g/L, C_0 = 5.0 mg/L and CT = 60 min).

It is known that at the isoelectric point or in other word, point of zero charge (pHpzc), surface charge of adsorbent is neutral, and in the pH values above pHpzc it has negative charge, whereas below pHpzc it is positively charged [24]. The obtained pHpzc for RHS was 6.6, where it was 6.1 for RRH and RB [25–28]. Predominant form of Pb(II) in the solution is Pb^{2+} at pH less than 6.0 and Pb(OH)$^+$ at pH 6.0–7.7 [23].

In this study the optimum pH for adsorption of lead was found to be at 6.0, which was lower than adsorbents' pHpzc. In the lower pHs competition between H$^+$ and the lead ions could diminish adsorption of lead ions. It is clear that the increase of solution pH reduces the competition between H$^+$

and the lead ions for binding sites with decreasing concentration of H+, favoring sorption at high *pH*. Therefore, when *pH* of the solution is around the pHpzc the best adsorption results were obtained, where the electrostatic repulsion is minimum between the positively charged lead ions and the surface [23]. Low adsorption of lead ions above *pH* value of 6.0 could be attributed to the precipitation of lead ions as hydroxide.

3.3. Effect of contact time

Optimization of the contact time (*CT*) was carried out for the maximum removal of Pb(II) on the adsorbents by changing agitating time in the reactor from 5 to 90 min. Based on the observed results (Fig. 4), the adsorption of lead consisted of two phases. The adsorption rate in the initial phase was immediate, while a relatively slow adsorption occurred in second stage. It sounds that, the first phase was external surface adsorption while the second one was the diffusion controlled adsorption [29,30]. When *CT* increased, pores of the sorbents were filled and the adsorption rate became slower and reached a plateau stage [31].

The adsorption increased from 15.7, 16.4 and 23.9% to 84.3, 73.6 and 91.9% respectively for RRH, RB and RHS, as the contact time was increased from 5 to 60 min. On further increase of *CT* up to 90 min, adsorption rate increased to 88.2, 76.3 and 93.6% but these increments were scant and slow specially for RHS. Hence, 60 min was considered to be the optimum *CT* for Pb(II) adsorption. The results declared that adsorption on RHS had a faster rate growth than the remains in the initial times and the adsorption mostly occurred in the first 30 min as the *RE%* of RRH, RB and RHS were 63.9, 59.4 and 78.5%, respectively.

3.4. Effect of adsorbent dosage

Dosages of the adsorbents were examined for the optimum value using 0.5, 1 and 2 g/L of the selected adsorbents. The results showed rapid increment of adsorption rate by increasing dose of adsorbents (Fig. 5). The increase in adsorption by adding adsorbent could be attributed to the larger surface area thereby increased number of binding sites available for Pb(II) [32]. Respectively for RRH, RB and RHS Pb(II) adsorption increased from 69.3, 63.3 and 74.8%
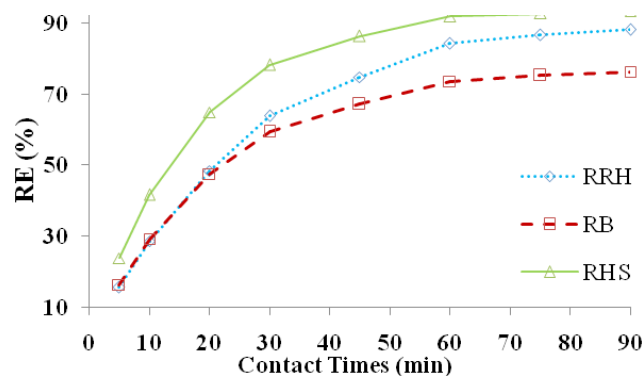
at dosage of 0.5 g/L to 88.2, 85.4 and 96.4% at dosages of 1.5 g/L.

Therefore, 1.0 g/L of the adsorbent was considered as an appropriate dosage for the remained examinations. The quick increment of adsorption with AD increase at the low dosages could be due to higher concentration gradient between the surface and pores of the sorbent and the bulk solution. So in higher dosage there are more free sites of adsorption for Pb ions and their adsorption decreases bulk concentration of Pb. This results in decrease of the concentration gradient and limits the concentration diffusion in the pores of the sorbent [27]. The significant decrease of *q* (mass of adsorbed Pb/mass of adsorbent) values with increasing dosage (Fig. 5) clearly shows less Pb uptake per unity of the sorbents is in consistent with above discussion.

3.5. Adsorption isotherm modelling

Adsorption isotherms provide valuable information on how the lead ions distribute between the solid and liquid phase at the equilibrium state of adsorption process. The information from the isotherms have a deterministic role to optimize the adsorption process [24].

The isotherm experiments were carried out with 1–15 mg/L of Pb concentrations, at solution *pH* 6.0 and the adsorbents' dosage of 1.0 g/L. The resulted data was analyzed by fitting to isotherm models including Langmuir, Freundlich, Redlich-Peterson (R-P), Temkin, Dubinin-Radushkevich (D-R) and Flory–Huggins (F-H).

3.5.1. Langmuir isotherm

In Langmuir model the basic supposition is that the sorption falls out at specific homogeneous sites through the adsorbent, and maximum adsorption corresponds to formation of a monolayer of adsorbate. Based on the assumptions of the isotherm, there is transmigration of adsorbate on the surface and adsorption energy is constant [33]. The mathematical form of Langmuir equation is presented as follows [34].

$$q_e = \frac{q_m K_L C_e}{1 + K_L C_e} \, linear \, form : \frac{C_e}{q_e} = \frac{1}{q_m} C_e + \frac{1}{K_L q_m} \qquad (2)$$

Fig. 4. Effect of contact time on lead removal efficiency ($pH_0 = 6$, *AD* = 1.0 g/L and C_0 = 5.0 mg/L).
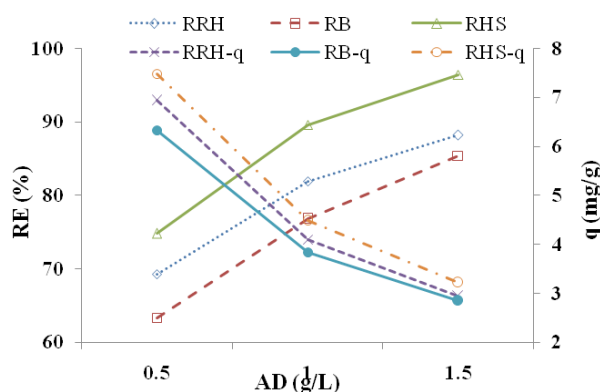
Fig. 5. Effect of adsorbent dosage on lead removal ($pH_0 = 6$, *CT* = 60 min, and C_0 = 5.0 mg/L).

where q_e is the equilibrium state adsorption capacity, which represents the amount of adsorbed lead per amount of adsorbent;

$$q_e = \frac{C_0 - C_e}{m} \qquad (3)$$

where C_0 is initial lead concentration (mol/L), C_e is equilibrium liquid phase concentration (mol/L), m is mass of adsorbent (g), q_m is maximum monolayer adsorption capacity (mol/g) and K_L is Langmuir constant related to energy of adsorption (L/mol), which corresponds to the concentration at which the amount of adsorbate bound to the sorbent is equal to $q_m/2$, and indicates the affinity of the adsorbate to bind with sorbent. Hence, a high K_L value indicates a higher affinity. Plotting C_e/q_e versus C_e gives a straight line with slop of $1/q_m$ and $1/K_L \cdot q_m$ which is its intercept. K_L and q_m were evaluated for the adsorption data from the slope and intercept of the plot, which are listed in Table 2; along with determination coefficient (R^2).

The results declared that maximum adsorption capacity and affinity of Pb to sorbent, given to the KL, for RHS (q_m = 15.6 mg/g, K_L = 188414 L/mol) is considerably more than RRH (q_m = 7.3 mg/g, K_L = 45078 L/mol) and RB (q_m = 4.8 mg/g, K_L = 123591 L/mol). This high adsorption capacity of RHS could be due to its more surface area (226.3 m²/g) [35] rather than RB (0.46 m²/g) [15] and RRH (2.48 m²/g) [25]. Also, a main portion of RHS is SiO_2 which its surface has commonly negative charge regarding the pHpzc of 6.6, that causes affinity to cations. It includes silanol (Si-OH),

Table 2
Determined constant values for the adsorption isotherms of lead ions on the selected adsorbents

		*Linear			Non-linear		
		RRH	RB	RHS	RRH	RB	RHS
Langmuir	K_L (L/mol)	45078	123591	188414	53377	186094	26974
	q_m (mg/g)	7.3	4.8	15.6	6.9	4.5	48.3
	R_L	0.39	0.26	0.066	0.36	0.2	0.14
	$-\Delta G^0$(KJ)	26.6	29.1	30.1	27.0	30.1	25.3
	R^2	0.96	0.96	0.73	0.98	0.92	0.99
	SE	0.138	0.235	0.054	1.7×10^{-6}	2.6×10^{-6}	2.9×10^{-6}
Freundlich	K_F (mol/g)(L/mol)$^{1/n}$	24.0×10^{-3}	3.0×10^{-3}	20.4×10^{-3}	5.1×10^{-3}	0.62×10^{-3}	494.0×10^{-3}
	$1/n$	0.68	0.49	0.53	0.54	0.35	0.77
	n	1.47	2.04	1.89	1.9	2.9	1.3
	R^2	0.96	0.87	0.98	0.97	0.85	0.99
	SE	0.147	0.300	0.158	2.0×10^{-6}	3.6×10^{-6}	2.4×10^{-6}
Redlich-Peterson	K_{RP} (L/g)	1.51	2.77×10^{29}	3.06×10^{29}	2.43	3.78	70
	a_{RP} (L/mol)$^{1/\beta}$	37180	9.11×10^{31}	1.5×10^{31}	8721	250551	151
	β	1	0.51	0.47	0.78	1	0.21
	$-\Delta G^0$ (KJ)	26.1	–	–	–	30.8	–
	R^2	0.94	0.88	0.97	0.98	0.92	0.99
	SE	0.2	0.16	0.09	2.2×10^{-6}	3.6×10^{-6}	3.3×10^{-6}
Temkin	K_T (L/mol)	685223	1783235	8995814	713449	1757353	8450306
	B	0.192	0.132	0.163	0.21	0.14	0.13
	b_T (kJ/mol)	12.9	18.8	15.2	14.7	17.1	19.9
	$-\Delta G^0$ (KJ)	33.3	35.7	39.7	33.4	35.6	39.5
	R^2	0.98	0.92	0.79	0.98	0.92	0.79
	SE	0.05	0.12	0.22	2.4×10^{-6}	3.8×10^{-6}	1.9×10^{-5}
D-R	q_m (mg/g)	104	38	127	55.38	18.96	933.06
	β	5×10^{-9}	3×10^{-9}	3×10^{-9}	3.9×10^{-9}	2.5×10^{-9}	5.6×10^{-9}
	E (kJ/mol)	10	12.9	12.9	11.3	14.2	9.5
	R^2	0.97	0.90	0.97	0.98	0.86	0.99
	SE	0.20	0.33	0.24	1.8×10^{-6}	3.4×10^{-6}	2.8×10^{-6}
F-H	K_{FH} (L/mol)	393	1250	1662	550	1500	2320
	n_{FH}	−5.95	−3.65	−1.33	−5.27	−3.26	−1.22
	$-\Delta G^0$ (KJ)	14.8	17.7	18.4	15.6	18.1	19.2
	R^2	0.87	0.92	0.92	0.93	0.89	0.99
	SE	0.28	0.25	0.19	9.5×10^{-6}	1.2×10^{-5}	9.8×10^3

*The graphs are presented in supplementary material (Fig. 3S–8S)

siloxane (Si-O-Si) and Si-O groups, which could contribute in ion-exchange reactions [36].

Owing to the great difference in the electronegativity of silicon and oxygen thereby the Si–O bond is fairly ionic, about 50% the ionic structure of silica provides a capability of adsorbing Pb ion [37]. Between RRH and RB, RRH showed more adsorption capacity (7.3 mg/g vs. 4.8 mg/g), which could be related to its more surface area, however affinity of RB (K_L = 123591) to Pb was higher than RRH (K_L = 45078).

The separation parameter (R_L) is a dimensionless equilibrium parameter of the Langmuir model which is given as follows:

$$R_L = \frac{1}{1 + K_L C_0} \tag{4}$$

For favorable adsorption process it is suggested that the value of R_L to lie in the range 0–1. R_L that indicates excellence and nature of adsorption, which as $R_L = 0$ for irreversible adsorption, $0 < R_L < 1$ for favorable adsorption, $R_L = 1$ for linear adsorption, and $R_L > 1$ for unfavorable adsorption [24,38].

The calculated R_L values for the adsorption of Pb onto RRH, RB and RHS respectively were 0.39, 0.26 and 0.066 which indicated favorable adsorption of Pb onto the sorbents. The non-linear form of the Langmuir isotherm was more consistent with the data from RRH and RHS (Table 2). The notable differences of the linear model were the higher adsorption capacity (48.3 mg/g) and RL (0.14) of RHS. The adsorption capacity (48.3 mg·g) in the present work is higher than the reported values of 10.86 [31] and 2.0 mg/g [39] for rice husk. It indicates agreeable performance of rice husk silica as an adsorbant substance.

3.5.2. Freundlich isotherm

Freundlich isotherm explains adsorption on both of homogeneous and heterogeneous surfaces [29]. It assumed a heterogeneous surface with a non-uniform distribution of adsorption heat over the surface and proposes that binding sites are not independent and/or equivalent. Following equation represents the isotherm. It could be applied for non-ideal adsorption on heterogeneous surfaces also multilayer adsorption [40].

$$q_e = K_F C_e^{\frac{1}{n}} linear\ form : \log q_e = \log K_F + \frac{1}{n}\log C_e \tag{5}$$

where K_F is the constant of Freundlich isotherm related to adsorption capacity and n is the constant of the isotherm related to the adsorption intensity. Plotting a graph of $log\ C_e$ vs. $log\ q_e$ gives straight line, and $1/n$ and $log\ K_F$ are slope and intercept of the line, respectively. The value of slope ($1/n$) shows the adsorption intensity or surface heterogeneity. As $1/n$ gets closer to 0 indicates that adsorbent is more heterogeneous and the value of $1/n$ close to or 1 indicates that adsorbent is a material with homogenous binding sites as is described by the normal Langmuir isotherm, whereas a value of $1/n$ above 1 is suggestive of cooperative adsorption [28, 34]. Also, n value of this isotherm is important regarding to description of adsorption given n as: $n = 1$ (linear); $n < 1$ (chemical process); $n > 1$ (physical process) [41] isotherm,

kinetic, mechanism and design equations for the analysis of adsorption in Cd (II).

For a favorable adsorption n value should be in the range 1–10 [42]. The constants of Freundlich isotherm and the related R^2 values were calculated and are recorded in Table 2. From Table 2, it is clear that n values were greater than 1, which indicate that the adsorption processes of Pb ions onto surface of the sorbents are favorable and follow the physical process. The values of $1/n$ showed more heterogeneous surface for RHS ($1/n$ = 0.49) than RRH ($1/n$ = 0.68), and R^2 values indicated well confidence of linear (R^2_{RHS} = 0.98, R^2_{RRH} = 0.96) and non-linear (R^2_{RHS} = 0.99, R^2_{RRH} = 0.97) Freundlich isotherm with adsorption of lead on RRH and RHS.

Evaluation of maximum adsorption capacity was regarding to the results of using various amounts of the adsorbents for a constant C_0. Thus, $log\ q_m$ was the extrapolated value of $log\ q$ for $C = C_0$. Then, given the Halsey equation [43] (Eq. (6)), the q_m was calculated and obtained 19.9, 14.7 and 12.9 mg/g respectively for RRH, RB and RHS.

$$K_F = \frac{q_m}{C_0^{1/n}} \tag{6}$$

3.5.3. Redlich-Peterson isotherm

Redlich–Paterson (R-P) is designated as a three parameter equation which is capable to represent adsorption equilibrium over a wide concentration range and due to its high versatility could be either applied in homogenous or heterogeneous systems [44]. This equation has the following form [45]:

$$q_e = \frac{K_{RP}C_e}{1 + a_{RP}C_e^{\beta}} linear\ form : \log\left(\frac{K_{RP}C_e}{q_e} - 1\right) = \beta \log C_e + \log a_{RP} \tag{7}$$

where K_{RP} is the R-P isotherm constant, a_{RP} is constant and β is a heterogeneity factor which lies between 0 and 1.

The isotherm is described by Eq. (6), and the constants in the equation could be evaluated from the obtained pseudo-linear plot by using a trial-and-error optimization method. In order to obtain the best value of K_{RP} which yields a maximum optimized value of R^2 [46], a trial-and-error procedure which is applicable to computer operations could be developed to determine the coefficient of determination, R^2, in series of values of K_{RP} for the linear regression of $log(C_e)$ on $log[(K_{RP}\ Ce/q_e) – 1]$.

Redlich and Paterson incorporated the characteristics of Langmuir and Freundlich isotherms into a single equation. Its behavior lines with the Freundlich isotherm in high concentrations. Where $K_F = K_{RP}/a_{RP}$ and $1/n = 1 – \beta$. Considering the heterogeneity factor β two limiting behaviours exist, i.e., Langmuir form for $\beta = 1$ and Henry's law form for $\beta = 0$ [47].

For $\beta = 1$ it reduces to the Langmuir equation, where $K_L = a_{RP}$, and $q_m = K_{RP}/a_{RP}$. For $\beta = 0$ it reduces to Henry's law as the following equation [48].

$$q_e = \frac{K_{RP}C_e}{1 + a_{RP}} \tag{8}$$

where $K_{RP}/1 + a_{RP}$ is the Henry's constant [49].

Evaluated constants of R-P isotherm are presented in Table 2. Consistent with the obtained heterogeneity factor

of Freundlich isotherm, RHS was the most heterogeneous adsorbent material with lower β (0.47) compared to RRH (β = 1) and RB (β = 0.51). The isotherm was reduced to Langmuir given the β value for RRH, which indicated the homogenous surface and monolayer adsorption of lead on RRH. Then for RRH K_L = a_{RP} = 37180 L/mol, which was fairly in accordance with the Longmuir isotherm (K_L = 45078 L/mol).

Although the non-linear form of the isotherm showed β = 1 for RB, but the fairly weak fitness (R^2 = 0.92) with the data don't permit to intend the obtained β. The non-linear R-P was more consistent with the results and estimated drastically different values for K_{RP} and a_{RP}. The resulted R^2 and SE inferred more reliability of non-linear R-P for the adsorption system. R-P isotherm was far from Henry's low limit for the examined sorbents when β was not close to 0 for them.

3.5.4. Temkin isotherm

The Temkin isotherm assumes linear decreasing for adsorption heat of all molecules in the layer with coverage due to adsorbent-adsorbate interactions. Also it presumes the characterization of adsorption by a uniform distribution of the binding energies; it considers maximum binding energy and declines the heat of sorption as a function of temperature, whereas it is linear rather than logarithmic, as implied in the Freundlich equation. This isotherm is commonly presented in the following form [24]:

$$\Psi = \left(\frac{RT}{b_T}\right)\ln\left(K_T C_e\right) linear\ form : \Psi = B\ln K_T + B\ln C_e \tag{9}$$

where $\Psi = q_e/q_m$ is fractional surface coverage, q_m obtained from linear Langmuir (see Table 2) for RRH and RB, and RHS q_m obtained from Freundlich (q_m = 12.9) according to reliability of their R^2 values. $B = RT/b_T$, and b_T is constant of Temkin isotherm related to heat of sorption (J/mol), K_T is the equilibrium binding constant corresponding to the maximum binding energy (L/g), R is the ideal gas constant (8.314 J/mol K), and T is the absolute temperature (K). K_T and B are determined by using the linear plot of Ψ vs $ln\ C_e$. The values of K_T, b_T and B are presented in Table 2.

Energy range for ion-exchange bonding mechanism is typically 8–16 kJ/mol and 20–40 kJ/mol for chemisorption, while physisorption processes are reported to have adsorption energies less than –40 kJ/mol [50]. The value of b_T indicates strong interaction between lead ions and the sorbents. Hence, the adsorption process of lead onto the sorbents could be expressed as ion-exchange. As indicated, the value of b_T adsorption mechanism in the RB was more close to chemisorption, but it was not in the range of 20–40 kJ/mol.

The non-linear model of the isotherm gives q_m values for RRH, RB and RHS, 8.1, 6.5 and 16.9 mg/g, respectively. This form of the equation was not more compatible with the results, but it included lower SEs. The predicted higher b_t (19.9 vs. 15.2 kJ/mol) for RHS was the main difference with the linear model.

3.5.5. Dubinin-Radushkevich isotherm

The adsorption data have been analyzed to distinguish the adsorption mechanisms based on the heterogeneous

characteristics of the adsorbents by using D-R isotherm. This model is generally used to describe the adsorption on a heterogeneous surface with a Gaussian distribution of adsorption energy [51].

There are some limitations for application of DR equation onto liquid-phase adsorption due to the complexities associated with other factors such as pH and ionic equilibrium intrinsic in aqueous solutions. Additionally, the non-ideal bulk solution often is rendered due to the solute-solvent interactions [52]. However, in many researches on adsorption of metal ions, this model is used to distinguish the adsorption mechanisms regarding to the mean free energy (E) of adsorption. In this regard, E is amount of energy that is required to drive a molecule from its location on the adsorbate to the infinity [51]. It could be evaluated with the following expression.

$$E = \left[\frac{1}{\sqrt{2\beta}}\right] \tag{10}$$

where β is the isotherm constant. It could be evaluated form the D-R isotherm as the mathematical expression of D-R model for the liquid phase system is expressed by the following equation.

$$q_e = q_m \exp\left(-\beta\varepsilon^2\right) linear\ form : \ln q_e = \ln q_m - \beta\varepsilon^2 \tag{11}$$

Meanwhile, the parameter ε can be correlated as [53]:

$$\varepsilon = RTln\left[1 + \frac{1}{C_e}\right] \tag{12}$$

The obtained results of D-R isotherm are presented in Table 2, the values of E show that the adsorption mechanisms for all three sorbents were in the range of ion-exchange process. The non-linear form of D-R predicted considerably higher q_m and fairly lower E for RHS. This form of the equation also fitted with the results of RRH and RHS and reliability of application for them.

3.5.6. Flory–Huggins isotherm

This model occasionally derives the degree of surface coverage characteristics of adsorbed substance onto adsorbent surface. It could declare the feasibility of adsorption, and spontaneous nature of an adsorption process. The F-H isotherm is expressed as the following formulation.

$$\frac{\theta}{C_0} = K_{FH}\left(1-\theta\right)^{n_{FH}} linear\ form : \log\left(\frac{\theta}{C_0}\right) = \log K_{FH} + n_{FH}\log n_{FH}\log(1-\theta) \tag{13}$$

where K_{FH} and n_{FH} are the indication of its equilibrium constant and model exponent. The equilibrium constant, K_{FH} could be used for the calculation of spontaneity free Gibbs energy [51,52]. In this equation, θ is the degree of surface coverage and is calculated as following:

$$\theta = 1 - \frac{C_e}{C_0} \tag{14}$$

The values of parameters for this isotherm are presented in Table 2. Non-linear forms of the model had better fitness with RRH and RHS but the SE of RHS were nota-

bly high. It was declared form the results that coverage (θ) were not considerably reduced for RHS, as a function of C_0, compared to the remains (Fig. 6). On the other hand, a sprightly increment of the area covered with the lead ions, [S, Eq. (15)], was seen for RHS. This could be due to the high surface area of RHS and its high affinity to lead ions which made it able to adsorb ions on the surface in higher concentrations of lead. However, the coverage was notably decreased for RB and RRH and the covered area with the lead ions did not increase significantly for them. This could be related to their very small surface area, than RHS, which could not support more adsorption capacity for the higher concentrations. The covered area with the lead ions estimated according to Eq. (15) [54].

$$S = \frac{q_e A \pi r^2}{M \times 10^3} \qquad (15)$$

where S (m^2/g) is the covered area of each gram of sorbents with the lead ions, $A = 6.022 \times 10^{23}$ is the Avogadro's number, $r = 4.01 \times 10^{-10}$ m is ionic radius of lead and $M = 207.2$ g/mol is the molar mass of lead.

3.6. Adsorption rate and kinetic

Adsorption of lead onto the selected sorbents firstly was investigated to find the most probable order of reaction and the using pseudo-first-order, pseudo-second-order, Bangham and intra-particle diffusion kinetic models. In this regard, adsorption investigation on the sorbents was carried out in a 250 ml bath reactor with $C_0 = 5$ mg/L, $pH_0 = 6$, $t = 5$–90 min and $AD = 1$ g/L as shown in Fig. 7.

3.6.1. The order of reaction

The reaction orders for adsorption of lead on RRH, RB and RHS were studied initially with the expression of [55]:

$$\log\left(\frac{-\Delta C_e}{\Delta t}\right) \simeq \log K + n \log \overline{C} \qquad (16)$$

where K is the reaction constant (min^{-1}), n is order of the reaction and (mg/L) is the mean concentration in the solution for Δt. Fig. 7 represents the obtained plot for the reactions and
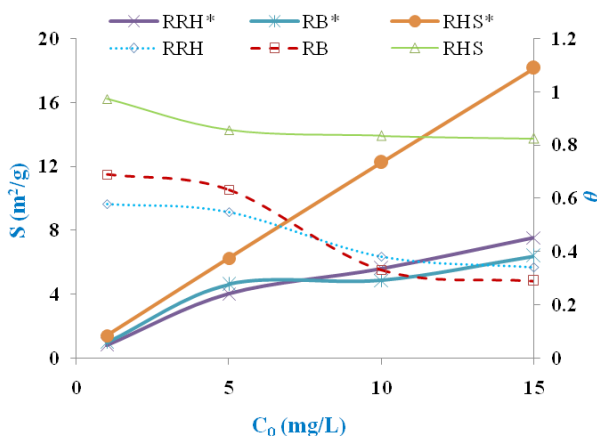
the reactions' constants. The most reaction constant of 0.026 min^{-1} was obtained for RHS. Also, it could be stated according to the plot that the adsorption reactions ($n_{RRH} = 1.6$, $n_{RB} = 2.7$, $n_{RHS} = 1.7$) were close to second and third order. Hence, given the obtained results for the rate of lead adsorption on the selected sorbents, pseudo-first and pseudo-second order reactions could be consistent expressions. The values of n indicate that pseudo-first order equation could be more reliable for RRH and RHS, while for RB the pseudo-second order equation sounds to be more compatible.

3.6.2. Rate constants of the adsorption

As discussed above, pseudo-first-order [Eq. (17)] and second-order rate equations [Eq. (18)] were applied to elaborate the rate of lead adsorption on the selected adsorbents. Eqs. (17) and (18) express the Lagergrens pseudo-first-order and pseudo-second order reaction, respectively [24,56].

$$\frac{dq_t}{d_t} = K_f\left(q_e - q_t\right) linear\ form : \log\left(q_e - q_t\right) = \log q_e - \frac{K_f}{2.303}t \qquad (17)$$

$$\frac{dq_t}{d_t} = K_s\left(q_e - q_t\right)^2 linear\ form : \frac{t}{q_t} = \frac{1}{K_s q_e^2} + \frac{1}{q_e}t \qquad (18)$$

In these equations q_t (mg/g) is the amount of lead adsorbed at time t. K_f (min^{-1}) is the pseudo first order rate constant, K_s is the pseudo second order rate constant (g/mg·min), t is the contact time (min) and $K_s q_e^2$ (mg/g·min) is expressed as initial adsorption rate (at $t \to 0$) [57]. The integration of the equations with initial condition ($q_t = 0$ at $t = 0$) leads to their linear form.

Half-life ($t_{1/2}$) of lead in the sorbents was estimated based on the obtained reaction constants. Below equations respectively denote the half-life for first and second order models [58,59]. The estimated values of the rate constants are presented in Table 3.

$$t_{1/2} = \frac{2.303}{K_f} \qquad (19)$$

$$t_{1/2} = \frac{1}{K_s q_e} \qquad (20)$$

Fig. 6. Coverage (θ) and occupied surface area (asterisks) of the selected adsorbents as a function of concentration (C_0).
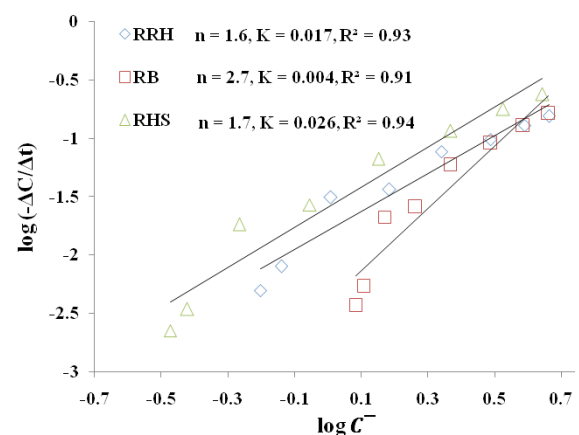
Fig. 7. Reaction order and constants of lead adsorption on the selected adsorbents.

Table 3
Determined rate and kinetic constants for adsorption of lead ions on the selected adsorbents

		RRH	RB	RHS
Pseudo first-order model	K_f (min^{-1})	0.0453	0.0487	0.0605
	q_e (cal.) (mg/g)	4.94	3.94	4.85
	$t_{1/2}$ (min)	50.8	47.3	38.1
	R^2	0.996	0.998	0.997
	SE	0.04	0.03	0.05
Pseudo second-order model	K_s (g/mg·min)	0.0053	0.0095	0.0113
	q_e (cal.) (mg/g)	6.13	4.87	5.64
	$t_{1/2}$ (min)	30.9	21.8	15.7
	h (mg/g·min)	0.1983	0.2236	0.3599
	R^2	0.991	0.995	0.995
	SE	0.52	0.50	0.42
Elovich model	a (mg/g·min)	0.44	0.47	0.73
	b (g/mg)	0.74	0.91	0.79
	R^2	0.990	0.988	0.973
	SE	0.15	0.14	0.23
Bangham model	α	0.0079	0.0068	0.0056
	K_0 (ml·L/g)	67.92	70.05	102.16
	R^2	0.72	0.68	0.65
	SE	0.165	0.153	0.147
Weber–Morris intra-particle diffusion model	K_{id} (mg/g·min$^{1/2}$)	0.52	0.42	0.47
	C (mg/g)	-0.04	0.29	0.75
	R^2	0.95	0.92	0.88
	SE	0.34	0.34	0.49

Regarding the R^2 values in Table 3, the results showed that the adsorption of lead on RRH, RB and RHS was superbly compatible with the pseudo first-order and pseudo second-order models. Appreciably more reaction constant (K) was found for RHS than the remains in both models. Given the R^2 and SE in Table 3, it is indicated that the results are most fitted with the pseudo first-order model. On the other hand, the lower half-lives were predicted for lead concentration via the pseudo second-order model which exerted more consistency with the experimental results which are presented in Table 3. Agreement of the results with the pseudo second-order reaction declares that the chemical adsorption is notably influenced the rate-limiting step of the adsorption [60]. Although the chemical bonding makes some difficulty to the recovery of sorbents, but it prevents form the secondary pollution to environment.

3.6.3. Elovich model

The Elovich model assumes heterogeneous nature for the solid surface active sites of sorbent and therefore, the sites exhibit different activation energies for chemisorption [61]. A kinetic principle is base of the model as it is assumed that with advance of adsorption the adsorption sites increase exponentially. Hence the model implies a multilayer adsorption [62].

Elovich equation is generally expressed as Eq. (21).

$$q_t = \frac{1}{b}\ln(ab) + \frac{1}{b}\ln t \tag{21}$$

where a is a constant of initial sorption rate of chemisorption (mg/g·min), and b represents extent of surface coverage (desorption constant) also it demonstrates activation energy of chemisorption (g/mg). a and b are evaluated from the linear plots of q_t vs $\ln t$. They are presented in Table 3 for the selected sorbents.

The pseudo first order, the pseudo second order and the Elovich model are based on the fact that the sorption is the rate limiting step in the adsorption process [54]. So, according to the results in the attributed table, the fitting to the models elucidated that the sorption was the leading cause of rate-controlling step. Also, the good fitness to the Elovich model indicated the multilayer adsorption of lead on the sorbents.

3.6.4. Bangham's equation

Bangham model supposes that the internal diffusion is the rate limiting step. Kinetic data were further used to know about the slow step occurring in the present adsorption system using Bangham's model as Eq.(22) [57].

$$\log\left(\frac{C_0}{C_0 - q_t m}\right) = \log\left(\frac{K_0 m}{2.303V}\right) + \alpha \log t \tag{22}$$
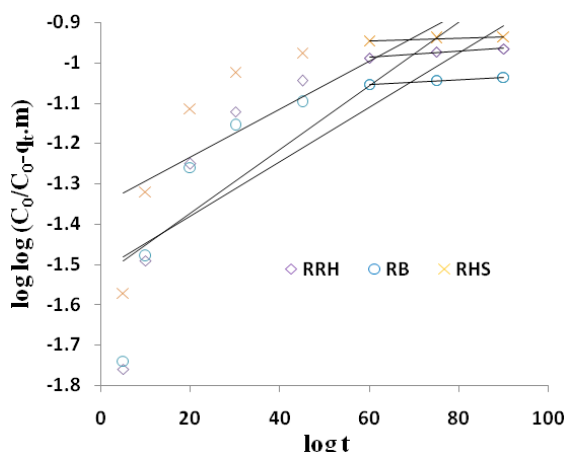
Fig. 8. Bangham's model plots for the removal of lead by the selected sorbents.

Fig. 9. Intra-particle diffusion plots for the removal of lead by the selected sorbents.

where V is the volume of the solution (ml), m is the weight of adsorbent per liter of solution (g/L). K_0(ml·L/g)and α (<1) are constants and are presented in Table 3. Plotting ($\log \log$ ($C_0/C_0-q_t m$) vs $\log t$) did not yield satisfactory linear curves for lead removal by the adsorbents. This demonstrated that the internal diffusion of adsorbate into pores of adsorbents is not the only rate-controlling step. Hence, the film and pore diffusion were important in the adsorption process. As the dependable straight lines (R^2_{RRH} = 0.98, R^2_{RB} = 0.99, R^2_{RHS} = 0.99) emerged when considering the end part of the process (60–90 min), one can state that the rate-controlling step of this part was the internal diffusion (see Fig. 8). This could be due to the diminished concentration gradient between the pores and bulk solution with increasing concentration of lead in the pores along with the process [63].

3.6.5. Weber–Morris intra-particle diffusion equation

The presented below expression describes Weber-Morris model [Eq. (23)], which is used to elucidate the influence of intra-particle diffusion on resistance to adsorption [24].

$$q_t = K_{id} t^{1/2} + C \tag{23}$$

In this model K_{id} is the intra-particle diffusion rate constant. A straight line passing the origin in the plot of q_t vs. $t^{1/2}$ indicates the compatibility of data with this model. Intercept of the line (C) represents thickness of the boundary layer, and the larger intercept shows the greater boundary layer effect [57]. Obtained values of the constants were accommodated in Table 3. Given the results the Weber-Morris model was fairly better fitted with data from RRH and RB than the Bangham's model (Fig. 9). This show partly influence of intra-particle diffusion on their adsorption rate rather than RHS. The deviation of straight lines from the origin indicates that the pore diffusion is not the only rate-controlling step. About RHS it may be caused by the difference between the rate of mass transfer in the initial and final stages of the adsorption. The first, sharper stage could be attributed to the diffusion of lead through the solution to the external surface of RHS or boundary layer
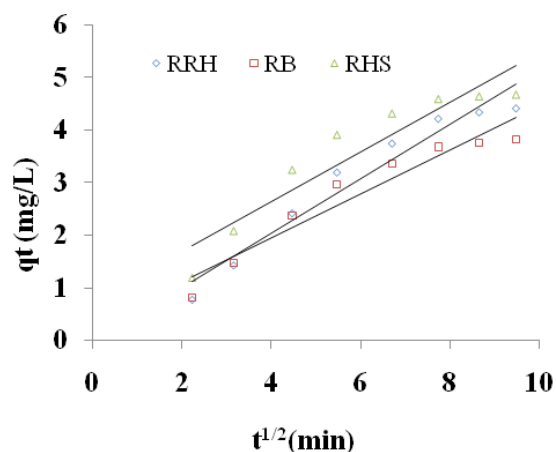
diffusion of solute molecules as the greatest C value was seen for the RHS up to 0.75 [63]. The straight lines obtained for the Bangham model for the selected adsorbents indicate that the intra-particle diffusion is the rate controlling step for the removal of lead ions.

3.7. Free energy of adsorption

The spontaneous nature of the on-going adsorption processes was examined by the change in Gibb's free energy ($\Delta G°$). It was calculated by using following equation:

$$\Delta G° = -RT \ln K \tag{24}$$

The values of K (L/mol) were obtained from Langmuir, R-P, Temkin and F-H isotherms. The results are presented in Table 2, which show the spontaneous nature of the adsorption by the sorbents and greatest values of $\Delta G°$ which were obtained for RHS (39.7 kJ/mol) from Temkin isotherm that was not so reliable given the R^2 of 0.79. $\Delta G°$, which in none of the cases was not reached the –40 kJ/mol as the energy of physisorption [50].

4. Conclusion

Regarding to the results of this study agricultural wastes of rice and especially RHS have appreciable capacity for adsorption of lead from an aqueous solution. Optimum pH for the adsorption of lead on the sorbent is obtained 6 and the optimum dosage of sorbent was 1 g/L with the contact time of 60 min. The adsorption of lead on RHS, RRH, and RB has include a spontaneous processes and ion-exchange determined as the dominant reaction.

The adsorption of lead on RRH, RB and RHS was fairly compatible with all examined isotherms, while non-linear Langmuir and non-linear R-P had the best fitness with the results. Subsequently, pseudo first-order model is in well agreement with the results of lead adsorption rate on the RHS, RRH and RB.

RHS showed the most adsorption capacity, high adsorption free energy and highest rate constants for adsorption

of lead compared to the RRH and RB. This indicated the effectiveness of the modification process on rice husk to get a better adsorbent.

Regarding the results, the boundary layer diffusions were the main rate-controlling steps of the adsorption of lead on the sorbents. About RHS the boundary layer diffusions was found to be more influencing factor in limiting the reaction rate compared to the remains.

Acknowledgements

References

[1] A. Andalib, H. Ganjidoust, B. Ayati, A. Khodadadi, Investigation of amount and effective factors on trihalomethane production in potablewater of Yazd, Iranian J. Health Environ., 4 (2011) 137–148.

[2] M. Kobya, E. Demirbas, E. Senturk, M. Ince, Adsorption of heavy metal ions from aqueous solutions by activated carbon prepared from apricot stone, Bioresour. Technol., 96 (2005) 1518–1521.

[3] A. Dąbrowski, Adsorption—from theory to practice, Adv. Colloid Interface Sci., 93 (2001) 135–224.

[4] N. Abdel-Ghani, M. Hefny, G.A. El-Chaghaby, Removal of lead from aqueous solution using low cost abundantly available adsorbents, Int. J. Environ. Sci. Technol., 4 (2007) 67–73.

[5] A. Jameel, A. Hussain, Removal of heavy metals from wastewater using activated rice husk carbon as adsorbent, Indian J. Environ. Protect., 29 (2009) 263–265.

[6] D. Mohan, C.U. Pittman, Arsenic removal from water/wastewater using adsorbents—a critical review, J. Hazard. Mater., 142 (2007) 1–53.

[7] E. Demirbas, M. Kobya, E. Senturk, T. Ozkan, Adsorption kinetics for the removal of chromium (VI) from aqueous solutions on the activated carbons prepared from agricultural wastes, Water SA, 30 (2004) p. 533–539.

[8] S.M. Mehdinia, P. Abdul Latif, A.M. Abdullah, H. Taghipour, Synthesize and characterization of rice husk silica to remove the hydrogen sulfide through physical filtration system, Asian J. Sci. Rec., 4 (2011) 246–254.

[9] S.M. Mehdinia, P. Abdul Latif, A. Makmom Abdullah, H.J.A.J.S.R. Taghipour, Synthesize and characterization of rice husk silica to remove the hydrogen sulfide through the physical filtration system, Asian J. Sci. Rec., 4 (2011) 246–254.

[10] M.V. Lopez-Ramon, F. Stoeckli, C. Moreno-Castilla, F. Carrasco-Marin, On the characterization of acidic and basic surface sites on carbons by various techniques, Carbon, 37 (1999) 1215–1221.

[11] S. Chandrasekhar, K.G. Satyanarayana, P.N. Pramada, P. Raghavan, T.N. Gupta, Review Processing, properties and applications of reactive silica from rice husk—an overview, J. Mater. Sci., 38 (2003) 3159–3168.

[12] N. Yalçin, V. Sevinç, Studies on silica obtained from rice husk, Ceram. Int., 27 (2001) 219–224.

[13] S.M. Mehdinia, P.A. Latif, H. Taghipour, Removal of hydrogen sulfide by physico-biological filter using mixed rice husk silica and dried activated sludge, Clean: Soil, Air, Water, 41 (2013) 949–954.

[14] V.G. Georgieva, M.P. Tavlieva, S.D. Genieva, L.T. Vlaev, Adsorption kinetics of Cr (VI) ions from aqueous solutions onto black rice husk ash, J. Mol. Liq., 208 (2015) 219–226.

[15] S. Montanher, E. Oliveira, M. Rollemberg, Removal of metal ions from aqueous solutions by sorption onto rice bran, J. Hazard. Mater., 117 (2005) 207–211.

[16] P. Jutzi, U. Schubert, Silicon Chemistry, Wiley-VCH, 2007.

[17] L. Ling, J. Li, G. Zhang, R. Sun, C.-P. Wong, Self-healing and shape memory linear polyurethane based on disulfide linkages with excellent mechanical property, Macromol. Res., 26 (2018) 365–373.

[18] U. Kalapathy, A. Proctor, J. Shultz, A simple method for production of pure silica from rice hull ash, Bioresour. Technol., 73 (2000) 257–262.

[19] N. Saxena, N. Pal, K. Ojha, S. Dey, A. Mandal, Synthesis, characterization, physical and thermodynamic properties of a novel anionic surfactant derived from Sapindus laurifolius, RSC Adv., 8 (2018) 24485–24499.

[20] N. Thuadaij, A.J.J.N.S.S.I.o.N. Nuntiya, Synthesis and characterization of nanosilica from rice husk ash prepared by precipitation method, J. Nat. Sci., 7 (2008) 59–65.

[21] V. Mastelaro, A.M. Flank, M.C.A. Fantini, D.R.S. Bittencourt, M.N.P. Carreño, I. Pereyra, On the structural properties of a-Si1–xCx:H thin films, J. Appl. Phys., 79 (1996) 1324–1329.

[22] M.S. Shafeeyan, W.M.A.W. Daud, A. Houshmand, A. Shamiri, A review on surface modification of activated carbon for carbon dioxide adsorption, J. Anal. Appl. Pyrolysis, 89 (2010) 143–151.

[23] L. Largitte, T. Brudey, T. Tant, P.C. Dumesnil, R. Lodewyckx, Comparison of the adsorption of lead by activated carbons from three lignocellulosic precursors, Microporous Mesoporous Mater., 219 (2016) 265–275.

[24] S. Kaur, S. Rani, R. Mahajan, M. Asif, V.K. Gupta, Synthesis and adsorption properties of mesoporous material for the removal of dye safranin: Kinetics, equilibrium, and thermodynamics, J. Ind. Eng. Chem., 22 (2015) 19–27.

[25] F. Mathew, Removal of heavy metals from electroplating wastewater using rice husk and coconut coir, in: Chemical Engineeing, Missouri University of Science and Technology, 2008, pp. 89.

[26] F. Adam, J.N. Appaturi, A. Iqbal, The utilization of rice husk silica as a catalyst: Review and recent progress, Catal. Today, 190 (2012) 2–14.

[27] V.S. Mane, I. Deo Mall, V. Chandra Srivastava, Kinetic and equilibrium isotherm studies for the adsorptive removal of Brilliant Green dye from aqueous solution by rice husk ash, J. Environ. Manage., 84 (2007) 390–400.

[28] F. Ogata, D. Imai, N. Kawasaki, Cationic dye removal from aqueous solution by waste biomass produced from calcination treatment of rice bran, J. Environ. Chem. Eng., 3 (2015) 1476–1485.

[29] T.A. Khan, S.A. Chaudhry, I. Ali, Equilibrium uptake, isotherm and kinetic studies of Cd (II) adsorption onto iron oxide activated red mud from aqueous solution, J. Mol. Liq., 202 (2015) 165–175.

[30] W. Zou, R. Han, Z. Chen, Z. Jinghua, J. Shi, Kinetic study of adsorption of Cu(II) and Pb(II) from aqueous solutions using manganese oxide coated zeolite in batch mode, Colloids Surf. Physicochem. Eng. Aspects, 279 (2006) 238–246.

[31] Q. Feng, Q. Lin, F. Gong, S. Sugita, M. Shoya, Adsorption of lead and mercury by rice husk ash, J. Colloid Interface Sci., 278 (2004) 1–8.

[32] S.A. Kosa, G. Al-Zhrani, M. Abdel Salam, Removal of heavy metals from aqueous solutions by multi-walled carbon nanotubes modified with 8-hydroxyquinoline, Chem. Eng. J., 181–182 (2012) 159–168.

[33] Y.C. Sharma, V. Srivastava, S.N. Upadhyay, C.H. Weng, Alumina nanoparticles for the removal of Ni(II) from aqueous solutions, Ind. Eng. Chem. Res., 47 (2008) 8095–8100.

[34] X. Liu, L. Zhang, Removal of phosphate anions using the modified chitosan beads: Adsorption kinetic, isotherm and mechanism studies, Powder Technol., 277 (2015) 112–119.

[35] S. Mehdinia, P. Latif, H. Taghipour, A comparative evaluation of dried activated sludge and mixed dried activated sludge with rice husk silica to remove hydrogen sulfide, Iran. J. Environ. Health Sci. Eng., 10 (2013) 1–7.

[36] R.M. Cavalcanti, W.A.G. Pessoa, V.S. Braga, I.D.L. Barros, Adsorption of sulfur compound utilizing rice husk ash modified with niobium, Appl. Surf. Sci., 355 (2015) 171–182.

[37] M. Ahmaruzzaman, Adsorption of phenolic compounds on low-cost adsorbents: a review, Adv. Colloid Interface Sci., 143 (2008) 48–67.

[38] K.R. Hall, L.C. Eagleton, A. Acrivos, T. Vermeulen, Pore- and solid-diffusion kinetics in fixed-bed adsorption under constant-pattern conditions, Ind. Eng. Chem. Fundam., 5 (1966) 212–223.

[39] D. Alexander, R. Ellerby, A. Hernandez, F. Wu, D. Amarasiriwardena, Investigation of simultaneous adsorption properties of Cd, Cu, Pb and Zn by pristine rice husks using ICP-AES and LA-ICP-MS analysis, Microchem. J., 135 (2017) 129–139.

[40] M. Hajjaji, H. El Arfaoui, Adsorption of methylene blue and zinc ions on raw and acid-activated bentonite from Morocco, Appl. Clay Sci., 46 (2009) 418–421.

[41] U.P. Kiruba, P.S. Kumar, C. Prabhakaran, V. Aditya, Characteristics of thermodynamic, isotherm, kinetic, mechanism and design equations for the analysis of adsorption in Cd (II) ions-surface modified Eucalyptus seeds system, J. Taiwan Inst. Chem. Eng., 45 (2014) 2957–2968.

[42] P.C. Mishra, R.K. Patel, Removal of lead and zinc ions from water by low cost adsorbents, J. Hazard. Mater., 168 (2009) 319–325.

[43] G.D. Halsey, The role of surface heterogeneity in adsorption, Adv. Catal., 4 (1952) e269.

[44] M. Belhachemi, F. Addoun, Adsorption of congo red onto activated carbons having different surface properties: Studies of kinetics and adsorption equilibrium, Desal. Water Treat., 37 (2012) 122–129.

[45] O. Redlich, D.L. Peterson, A useful adsorption isotherm, J. Phys. Chem., 63 (1959) 1024–1024.

[46] Y.-S. Ho, W.-T. Chiu, C.-C. Wang, Regression analysis for the sorption isotherms of basic dyes on sugarcane dust, Bioresour. Technol., 96 (2005) 1285–1291.

[47] J. Febrianto, A.N. Kosasih, J. Sunarso, Y.-H. Ju, N. Indraswati, S. Ismadji, Equilibrium and kinetic studies in adsorption of heavy metals using biosorbent: a summary of recent studies, J. Hazard. Mater., 162 (2009) 616–645.

[48] V.S. Mane, I.D. Mall, V.C. Srivastava, Kinetic and equilibrium isotherm studies for the adsorptive removal of Brilliant Green dye from aqueous solution by rice husk ash, J. Environ. Manage., 84 (2007) 390–400.

[49] H. Shahbeig, N. Bagheri, S.A. Ghorbanian, A. Hallajisani, S. Poorkarimi, A new adsorption isotherm model of aqueous solutions on granular activated carbon, World J. Modell. Simul., 9 (2013) 243–254.

[50] B. Kiran, A. Kaushik, Chromium binding capacity of Lyngbya putealis exopolysaccharides, Biochem. Eng. J., 38 (2008) 47–54.

[51] K.Y. Foo, B.H. Hameed, Insights into the modeling of adsorption isotherm systems, Chem. Eng. J., 156 (2010) 2–10.

[52] J. Febrianto, A.N. Kosasih, J. Sunarso, Y.-H. Ju, N. Indraswati, S. Ismadji, Equilibrium and kinetic studies in adsorption of heavy metals using biosorbent: A summary of recent studies, J. Hazard. Mater., 162 (2009) 616–645.

[53] V.K. Gupta, A. Mittal, A. Malviya, J. Mittal, Adsorption of carmoisine A from wastewater using waste materials—bottom ash and deoiled soya, J. Colloid Interface Sci., 335 (2009) 24–33.

[54] L. Largitte, T. Brudey, T. Tant, P.C. Dumesnil, P. Lodewyckx, Comparison of the adsorption of lead by activated carbons from three lignocellulosic precursors, Microporous Mesoporous Mater., (2015).

[55] L.D. Benefield, B.L. Weand, J.F. Judkins, Process chemistry for water and wastewater treatment, Prentice-Hall, Englewood Cliffs, N.J., 1982.

[56] A. Mittal, D. Kaur, A. Malviya, J. Mittal, V. Gupta, Adsorption studies on the removal of coloring agent phenol red from wastewater using waste materials as adsorbents, J. Colloid Interface Sci., 337 (2009) 345–354.

[57] I.D. Mall, V.C. Srivastava, N.K. Agarwal, I.M. Mishra, Removal of congo red from aqueous solution by bagasse fly ash and activated carbon: kinetic study and equilibrium isotherm analyses, Chemosphere, 61 (2005) 492–501.

[58] M. Alkan, Ö. Demirbaş, M. Doğan, Adsorption kinetics and thermodynamics of an anionic dye onto sepiolite, Microporous Mesoporous Mater., 101 (2007) 388–396.

[59] M. Doğan, H. Abak, M. Alkan, Adsorption of methylene blue onto hazelnut shell: Kinetics, mechanism and activation parameters, J. Hazard. Mater., 164 (2009) 172–181.

[60] L. Cui, L. Hu, X. Guo, Y. Zhang, Y. Wang, Q. Wei, B. Du, Kinetic, isotherm and thermodynamic investigations of Cu^{2+} adsorption onto magnesium hydroxyapatite/ferroferric oxide nano-composites with easy magnetic separation assistance, J. Mol. Liq., 198 (2014) 157–163.

[61] S. Chowdhury, R. Mishra, P. Saha, P. Kushwaha, Adsorption thermodynamics, kinetics and isosteric heat of adsorption of malachite green onto chemically modified rice husk, Desalination, 265 (2011) 159–168.

[62] O. Hamdaoui, E. Naffrechoux, Modeling of adsorption isotherms of phenol and chlorophenols onto granular activated carbon: Part I. Two-parameter models and equations allowing determination of thermodynamic parameters, J. Hazard. Mater., 147 (2007) 381–394.

[63] U.R. Lakshmi, V.C. Srivastava, I.D. Mall, D.H. Lataye, Rice husk ash as an effective adsorbent: Evaluation of adsorptive characteristics for Indigo Carmine dye, J. Environ. Manage., 90 (2009) 710–720.

Supplementary material

The BET value obtained for the surface area of rice husk silica was 226.3 m²g⁻¹. It shown to be mesoporous with a median pore radius of 2.4 nm. The BET parameter graphs are presented in Fig. 1S and 2S. Also, various isotherm for adsorption of lead ions on the selected adsorbents, RRH (row rice husk), RB (rice bran) and RHS (rice husk silica) are presented in Figs. 3S–8S.
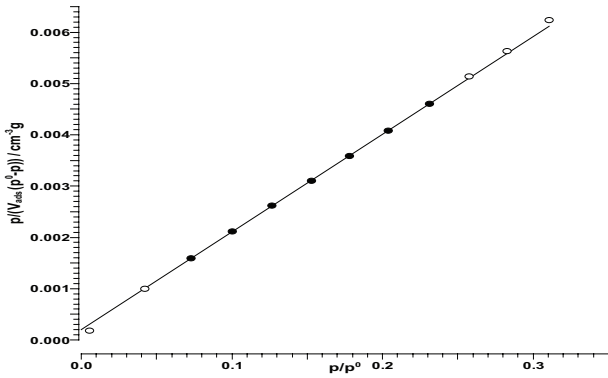
Fig. 1S. The BET surface area analysis, 2 parameters line (p/pᵒ) vs. $p/(V_{ads}(p^o–p))/cm^{-3}$ g in the Rice Husk Silica.
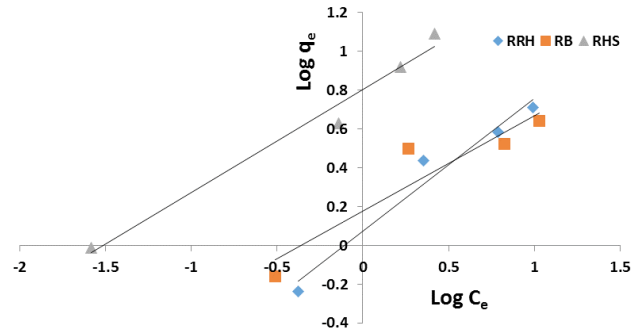
Fig. 4S. Freundlich isotherm graphs for the selected adsorbents.
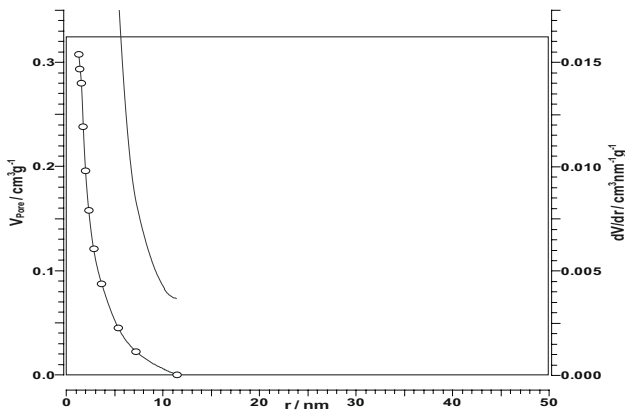
Fig. 2S. Pore radius size (nm) vs. pore volume (cm³ g⁻¹) in the Rice Husk Silica.
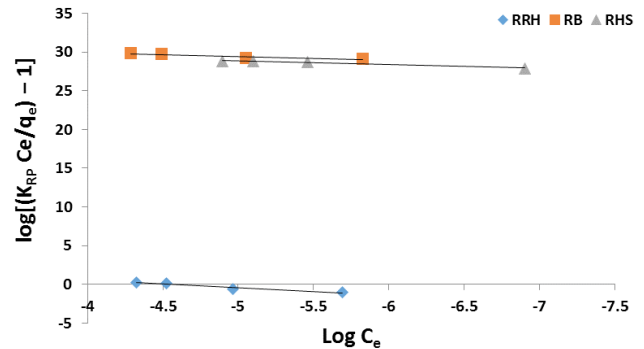
Fig. 5S. Redlich-Peterson isotherm graphs for the selected adsorbents.
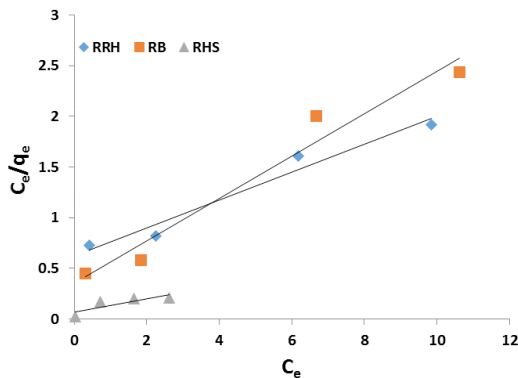
Fig. 3S. Langmuir isotherm graphs for the selected adsorbents.
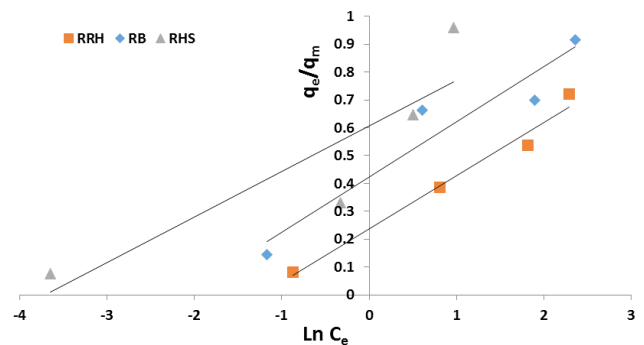
Fig. 6S. Temkin isotherm graphs for the selected adsorbents.
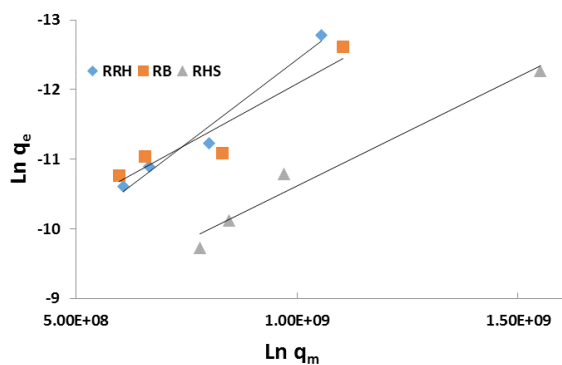
Fig. 7S. Dubinin-Radushkevich isotherm graphs for the selected adsorbents.
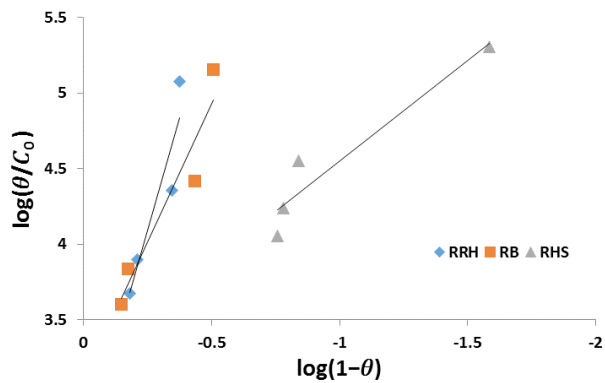
Fig. 8S. Flory–Huggins isotherm graphs for the selected adsorbents.